Spectral response of scintillating fibres

Z. Papandreou *, B.D. Leverington and G.J. Lolos

Department of Physics, University of Regina, Regina, SK, S4S 0A2, Canada

Abstract

The spectral response of PHT-0044 (blue) and BCF-20 (green) scintillating fibres was measured as a function of wavelength using a UV LED. It was observed that significant spectral strength from the PHT-0044 fibres was missing compared to manufacturer's specifications at the origin of the source, shifting the peak value of the spectrum to significantly higher values in wavelength. In contrast, the corresponding shift for the BCF-20 fibres was minimal. The mechanisms responsible for the observed behavior are discussed herein. Moreover, the attenuation length for each fibre type was extracted and studied as a function of wavelength. Finally, the measured fibre spectra were convolved with the wavelength response from a typical bi-alkali photo multiplier as well as a green-sensitive silicon photo multiplier and compared.

Key words: scintillating fibres, wavelength response, optical transmission, electromagnetic calorimeter
PACS: 29.40.Mc, 29.40.Vj

1 Introduction

The study in this paper was undertaken in the context of determining the optimal type of scintillating fibres to be coupled to the electronic front-end readout of the electro-magnetic barrel calorimeter (BCAL) for the GlueX project. This experiment aims to elucidate *confinement* in Quantum Chromodynamics, by searching for hybrid mesons that possess gluonic degrees of freedom and exotic quantum numbers, and arise from photoproduction at 9 GeV [1,2]. To achieve this goal, amplitude analyses on numerous exclusive reactions must be carried out to determine the J^{PC} quantum numbers of produced exotic mesons, which decay into photons and charged particles. Clearly, an overall

* Corresponding author. Tel.: +1 306 585 5379; fax: +1 306 585 5659
Email address: `zisis@uregina.ca` (Z. Papandreou).

hermetic detector with adequate resolution is essential, and the BCAL is a crucial subsystem. Indeed, this calorimeter will cover 11° to 126° with respect to the beam direction, and will be charged primarily with the detection of photons resulting from $\pi^0 \to \gamma\gamma$ and $\eta \to \gamma\gamma$ decays in the 40 MeV to 4 GeV energy range.

The BCAL is a sampling calorimeter based on scintillating fibres and will be deployed inside the GlueX detector's super-conducting solenoid. The central field of the solenoid is 2.2 T, resulting in substantial magnetic field strength and gradients near the BCAL ends, so using vacuum PMT's with short light guides is not possible. The leading option is to use silicon photomultipliers (SiPM) coupled to compact light guides. These devices are immune to large magnetic fields and typically have their peak quantum (QE) and photon-detection (PDE) efficiencies in the green optical region. Our collaboration has been working with SensL [1] to develop large-area (1.26 cm^2) SiPM arrays (SiPMPlus), based on sixteen 3×3 mm^2 cells with each cell having $\sim$3 600 pixels. These devices will match the GlueX readout cell size of $\approx 2 \times 2$ cm^2 for the inner 12 cm, in depth, in a 4×6 segmentation pattern. The outer 10 cm will be read out using fine-mesh PMTs in a 2×2 segmentation pattern and readout area of $\approx 5 \times 5$ cm^2.

The BCAL will be comprised of a lead and scintillating fibre matrix, consisting of $\sim$200 layers of lead sheets, each of 0.5 mm thickness, and 1-mm-diameter, multi-clad, scintillating fibres (SciFi), bonded in place using BC-600 optical epoxy [2]. This geometry results in $\sim$18 000 fibers per module. The detector will consist of 48 modules each $\sim$ 4 cm long and with a trapezoidal cross section, and will form a cylindrical shell with inner and outer radii of 65 cm and 90 cm, respectively. The simulated sampling fraction – fraction of photon energy deposited in the SciFi's with respect to the total energy deposited in the module – is 12.5%. Two full-sized prototype modules were constructed: Module 1 was built entirely of PHT-0044 [3] fibres, whereas Module 2 was built with a combination of PHT-0044 and BCF-20 fibres.

The chemical and optical properties of scintillating materials have been presented elsewhere [3–5]. Such materials are composed of a chemical base, usually polystyrene or polyvinyltoluene, and one or more dyes that are added to improve the quantum yield of the scintillator and to waveshift the scintillation light to longer wavelengths. The attenuation length depends on the self-absorption of the materials and reflection losses as the photons travel down the fibre [6]. This is illustrated in manufacturer's absorption and emission spectra for the second dye in BCF-12 and BCF-20 as shown in Fig. 1, together with

[1] SensL, Blackrock, Cork, Ireland (www.sensl.com)
[2] St. Gobain Crystals & Detectors, Hiram, OH 44234, USA (www.bicron.com)
[3] PolHiTech SRL, 67061 Carsoli (AQ), Italy (www.polhitech.it)

the stimulated wavelengths from the two light sources used in our experiment. The overlap between the absorption and emission spectra in Fig. 1 is minimal, thus resulting in long attenuation length for these fibres. The integral of the transmitted light intensity decreases linearly as a function of the distance that the light travels in the fibre, i.e. there is an exponential loss of photons. The various wavelength regions exhibit differing slopes in these curves, with the shorter wavelengths following steeper slopes [3].

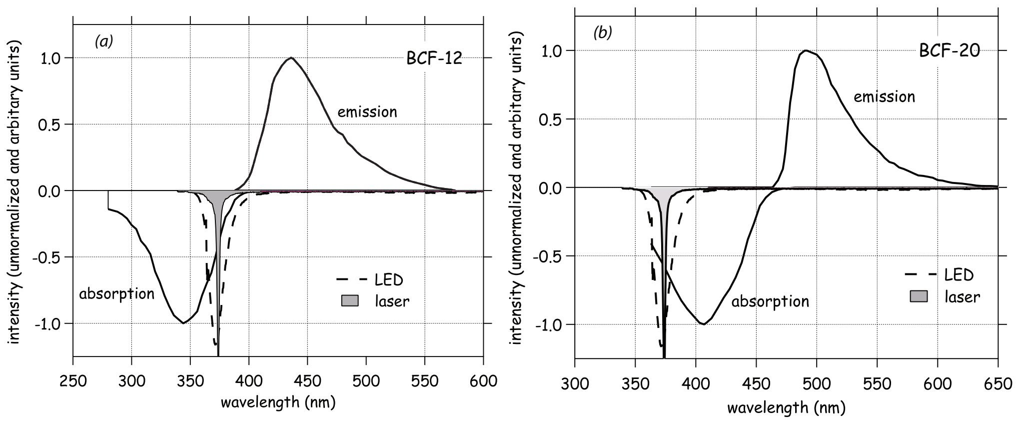

Fig. 1. Emission and absorption spectra from the secondary dye of (a) BCF-12 and (b) BCF-20 fibres. Although BCF-12 fibers were not used in this study, their spectrum is similar to other blue-emitting fibers such as the PHT-0044 used herein, and is shown here for qualitative purposes. Also displayed are the stimulated wavelength ranges from the 373 nm LED and 375 nm laser used in our measurements, as discussed below. All curves have been arbitrarily normalized to facilitate the comparison of their spectral shapes.

In this paper, our investigation focused on the measurement of wavelength spectra from 1-mm-diameter PHT-0044 and BCF-20 SciFi and the subsequent analysis to extract the short- and long-attenuation lengths as well as the dependence of the attenuation length on wavelength. Both SciFi types are composed of a core of polystyrene and two layers of polymethylmethacrylate cladding: the first from acrylic and the second from fluor-acrylic material, having thicknesses of 3% and 1% of the fibre's diameter[4]. An important issue in the data analysis is the normalization of the light produced at the source, corresponding to near-zero fibre length. To this end, manufacturers' source spectra were examined and compared to our nearest measurements (1 mm fibre length). The properties of PHT-0044 and BCF-12 are quite similar, in terms of peak emission and attenuation length. Source spectra are not available for the former, and this is why the BCF-12 spectra were used, instead.

The breakdown of this paper is as follows. The experimental measurements are described in Section 2, the data analysis is presented in Section 3 and the conclusions in Section 4.

[4] St. Gobain Crystals & Detectors, Scintillating Optical fibres Brochure 605.

2 Measurements

For the measurements reported herein, a LED light source, a spectro-photometer and the tested SciFi were coupled together in a robust and reproducible manner. The SD2000 dual-channel fibre optic spectro-photometer [5] is based on a blazed diffraction grating with a 50 μm wide slit and features a high-sensitivity 2048-element linear CCD array that provides high response and excellent optical resolution from 200-1100 nm. This device had been calibrated by the manufacturer, and the provided specifications indicated a wavelength difference, $|\delta\lambda|$, between expected and measured values, never exceeding 0.3 nm for any given pixel on the CCD. The SD2000 employs an external ADC1000-USB A/D converter to communicate with a PC running commercial software. The spectro-photometer had an integration window of 150 μs and measured the wavelength region of 340-1020 nm in over 2000 bins, resulting in a resolution of $\sim$3.3 bins/nm (or 0.3 nm). As a result, although the spectral shapes appear jagged at each wavelength, upon close inspection the overall behavior of the data was stable, as evidenced by their long-wavelength tails that overlapped above 500 nm as expected, since at those wavelengths there is little absorption of light. This feature will be demonstrated below. Sample dark spectra were obtained and these had negligible effect on the measured spectra with UV light.

For our measurements, a RLU370-1.7-30 ultra violet LED [6] was employed, with a peak emission wavelength of 373 nm, a spectrum bandwidth of 13 nm, and typical radiant flux of 1.7 mW. Selected measurements were also performed using a 375 nm PicoQuant PDL 800-B picosecond pulsed diode laser with LDH-P-C-375B laser head [7]. A comparison of the spectra from the LED and the laser, as measured directly with the spectro-photometer, are shown in Fig. 2. These demonstrate that: a) the spectro-photometer had been correctly calibrated versus wavelength by its manufacturer, since the peak emission of the LED and the laser indeed were measured to be at 373 nm and 375 nm, respectively, and the peak widths were 13 ns and 1 ns, in agreement with manufacturers' specifications; b) There is no significant contribution from these light sources to the intensity of the measured fibre spectra in the wavelength range of interest, since the broad LED peak at $\sim$560 nm is only at the few percent level and does not fall in the excitation region of the fibres. In any case, this peak does not appear in the fibre spectra when the LED is positioned perpendicularly to the tested SciFi. The spectro-photometer was also used to measure the spectra of other LEDs at 470 nm and 590 nm and was found equally accurate.

[5] Ocean Optics Inc., Dunedin, FL, USA (www.oceanoptics.com)
[6] Roithner Lasertechnik,Vienna, Austria (www.roithner-laser.com)
[7] PicoQuant GmbH, Berlin, Germany (www.picoquant.com)

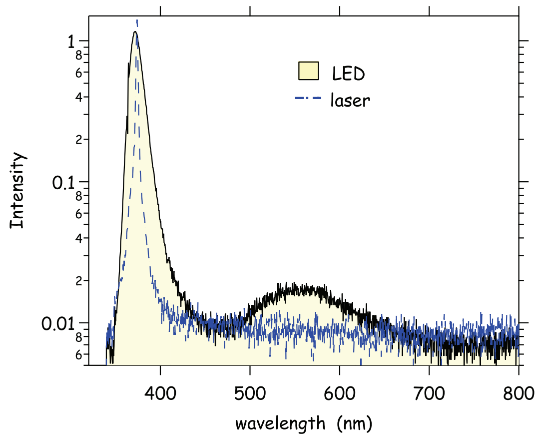

Fig. 2. Comparison of the emission spectra of the LED and the laser as measured directly, using the spectro-photometer, and plotted on a logarithmic scale. Details are provided in the text. (colour online)

The fibre under test was clamped in place horizontally until it was taut, with one end held via a clamp on a lab stand while the other was glued through a SMA connector using BC-600 epoxy. Once the glue had cured, the fibre end at the tip of the SMA connector was polished using three progressive grades of polishing paper (coarse, 12 μm and 3 μm grit) and a polishing puck, from a Clauss [8] fibre Optic Polishing kit (PK-2000), and was cleaned using ethyl alcohol and KimWipes to remove metallic dust originating from the tip of the SMA connector. Finally, the SMA end was coupled to the spectro-photometer's slave channel. This method allowed for easy and reproducible coupling of fibre to spectro-photometer. The setup was made robust to protect against displacing the test fibre and was leveled to avoid any curvature in the test fibres.

The LED was installed in a commercial housing and was mounted on a specially designed stand that could slide on the lab bench and translated across the length of the fibre (from 8 cm to 380 cm) in a parallel fashion, guided by a set of aligned, steel ruled guides. A schematic drawing of the setup is shown in Fig. 3. It should be noted that in that figure the distance of the LED housing port (P) to each fibre tested was 3 mm and held constant to maintain a consistent beam profile. With this setup, relative comparisons of the measured light intensity along the length of a given fibre were possible. However, due to the different level of polish of each fibre, absolute comparisons from one fibre to another were not possible as far as the measured intensity went, although the spectral shapes were unaffected and could still be compared.

All measurements were carried out in complete darkness in our lab. However, since the core of blue-emitting scintillating fibres can be damaged by prolonged

[8] The PK-2000 can be obtained from a large number of fibre accessories vendors.

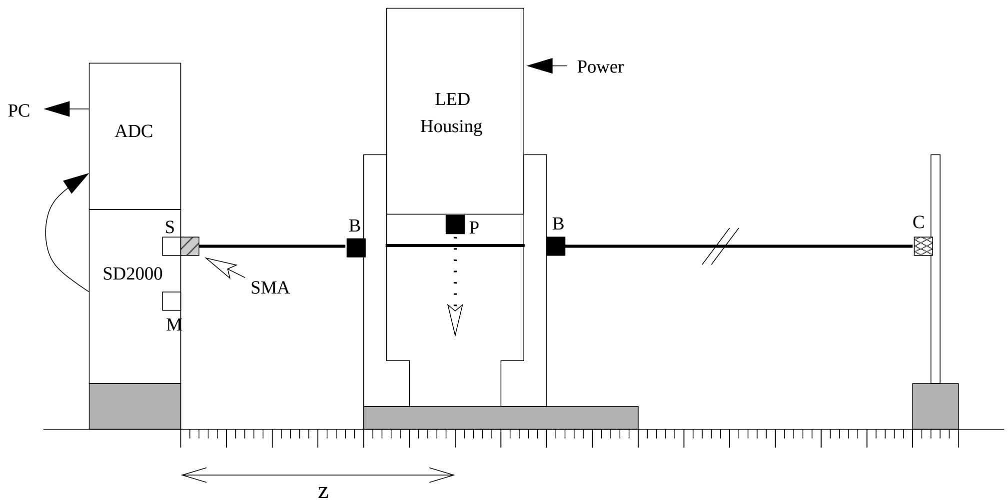

Fig. 3. Schematic drawing of the experiment. The test fibre is shown as the bold horizontal line: on the right it is clamped to a lab stand (C), in the middle it threads through the legs of the LED support stand via barrels (B) having 1 mm inner diameter holes and external threads that mount on the support frame and on the left it is connected to the slave channel (S) of the SD2000 spectro-photometer by an SMA connector. The SD2000 connects to the ADC via a flat-ribbon bus and the ADC, in turn, connects to a PC via a USB cable. The vertical arrow pointing downwards from the LED housing indicates the direction of the incident light through its port (P) onto the test fibre. The horizontal displacement of the light direction to the entrance of the SD2000 master channel is our distance parameter, z. This figure is not to scale: for example, the LED's port is a lot closer to the fibre than implied in this schematic.

exposure to UV light, yellow, UV-absorbing film (TA-81-XSR[9]) was used to cover all fluorescent overhead and incandescent desk lights in our detector test laboratory during the preparation and setup stages.

3 Results

This section is subdivided as follows. The fitting of the wavelength spectra for distances from 8 cm to 380 cm is presented first, since this method was entirely self consistent and independent of assumptions on the manufacturer's source (0 cm) spectra. This is followed in sequence by a different set of measurements from 1 mm to 20 mm and a comparison of those results to manufacturer's spectra. Finally, the effect of two different photosensors on the measured spectra is shown.

[9] Window Film Systems, London, ON, Canada (www.windowfilmsystems.com)

3.1 *Fitting the emission spectra*

The measured spectra for the BCF-20 are well described by a Moyal function plus a flat background:

$$f(x, a, \mu, \sigma, b) = a \cdot \exp\left(-\frac{1}{2}\left(\frac{(\lambda-\mu)}{\sigma} + e^{-(\lambda-\mu)/\sigma}\right)\right) + b. \quad (1)$$

On the other hand, the PHT-0044 fibre spectra require a sum of two Moyal functions plus a flat background. The Moyal distribution is often used as a good approximation to the Landau distribution [7], and was chosen here as the description with the fewest fit parameters; in any case, it was employed simply as a tool to integrate the spectra and proceed further in the analysis. The results of fits to Moyal functions for spectral measurements at LED distances ranging from 8 to 380 cm for both fibre types are shown in Fig. 4.

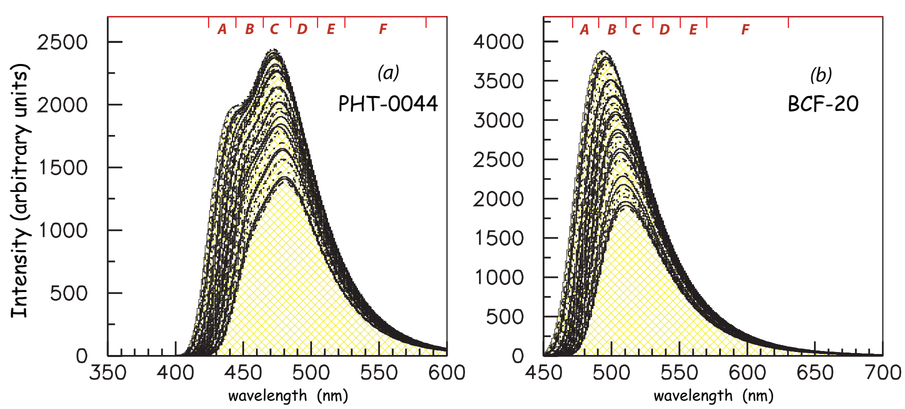

Fig. 4. The results of fits to Moyal functions for spectral measurements at source distances ranging from 8 to 380 cm for (a) PHT-0044 and (b) BCF-20 fibres. The wavelength ranges labeled A through F in the plots will be referenced later in this paper. (colour online)

The single Moyal function fits have 4 parameters including an amplitude (a), a characteristic wavelength and width (given by μ and σ) and the background term (b). The fits involving a sum of two Moyal functions introduce three additional parameters. The BCF-20 fibre spectral fits are characterized by a single wavelength (μ) and width (σ) and the PHT-0044 fits are characterized by two wavelengths (μ_1 and μ_2) and corresponding widths (σ_1 and σ_2). The dependence of these fit parameters on LED distance is shown in Fig. 5. The integral of the background term over wavelength from 400 to 700 nm is about 5% of the integral of the spectra over this same wavelength range.

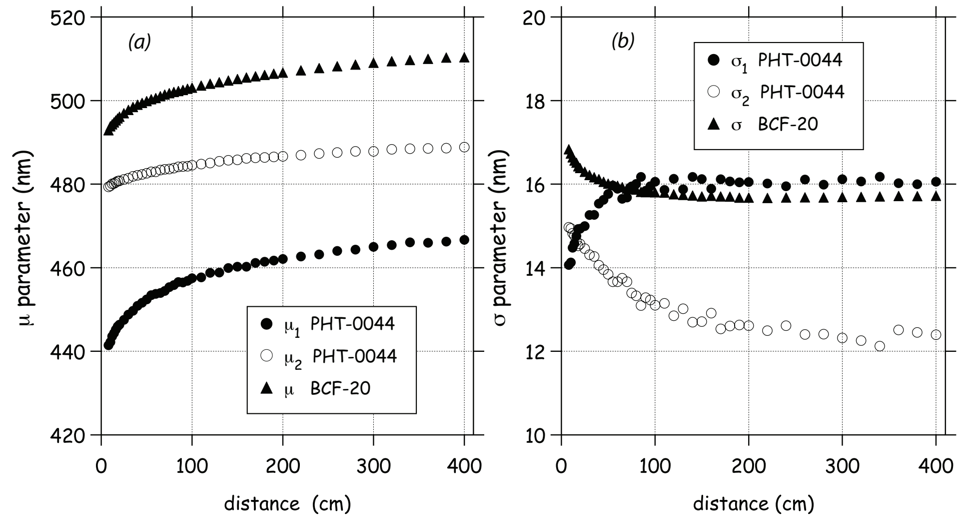

Fig. 5. Dependence of the Moyal fit parameters (a) μ and (b) σ as a function of source distance for the PHT-0044 and BCF-20 fibres.

3.2 Attenuation length versus wavelength

The Moyal fits described above were integrated over wavelength for the two fibres for various source distances. Six ranges of wavelength (labeled A through F) over which the integrals were performed are indicated in Fig. 4 for the two fibres. The central (middle of each bin) wavelengths are indicated in the legend of the plots in Fig. 6. These data were fit to an exponential of the form:

$$I(d) = I_0 + \alpha \cdot e^{-(d-d_0)/\lambda} \tag{2}$$

For the fits shown, the floor term was set at about 10% of the maximum value for the data in a particular wavelength range. Without the inclusion of a floor term consistent single-exponential fits could not be obtained; this term does not originate from a spectrophotometer calibration but is most likely due to spectrum fluctuations as a result of the method of illuminating the fibers. The d_0 was not a fit parameter but rather was determined by the starting point of the fit which was $d_0 = 8$ cm for all the wavelength ranges except for the wavelength range labeled A, which required a $d \geq 8$ cm in order to obtain a good quality fit due to the rapid absorption at small wavelengths. The fit parameter λ is the attenuation length and its dependence on wavelength for the two fibres is shown in the left panel of Fig. 7. Such behaviour was first reported in reference [3].

The attenuation lengths in the right panel of Fig. 7 were obtained by plotting the value of the Moyal fit function as a function of distance at discrete wavelengths and fitting to an exponential. Note the structure in this dependence around 460 nm to 470 nm that corresponds to the region of the second peak in

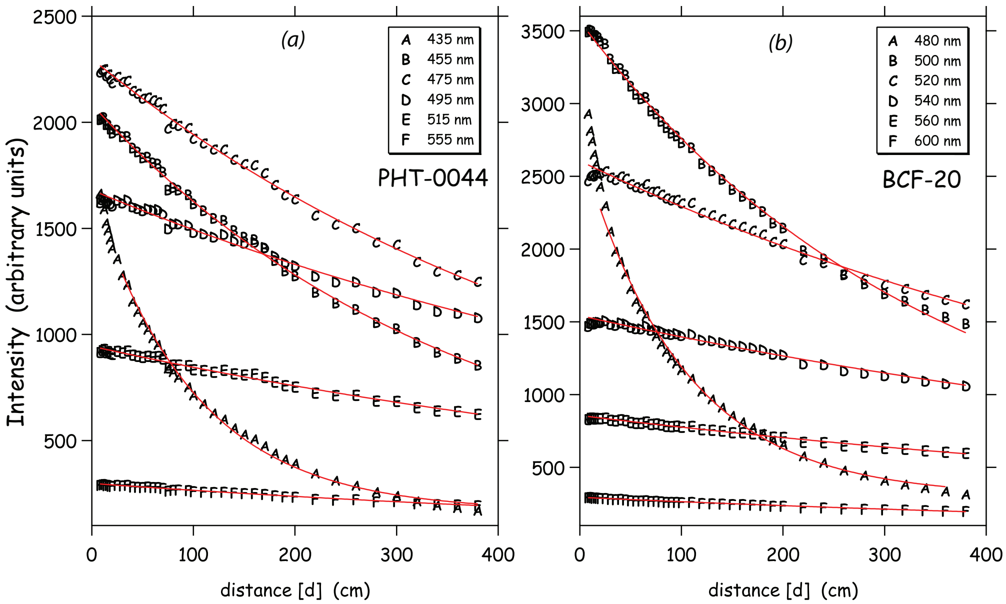

Fig. 6. Integrals of the Moyal fits to the fitted data are shown as a function of source distance for (a) the PHT-0044 and (b) the BCF-20 fibres. The points labeled A through F are the integrals for the wavelength ranges defined in Fig. 4. The curves are results of fits to a single exponential. More details are given in the text.

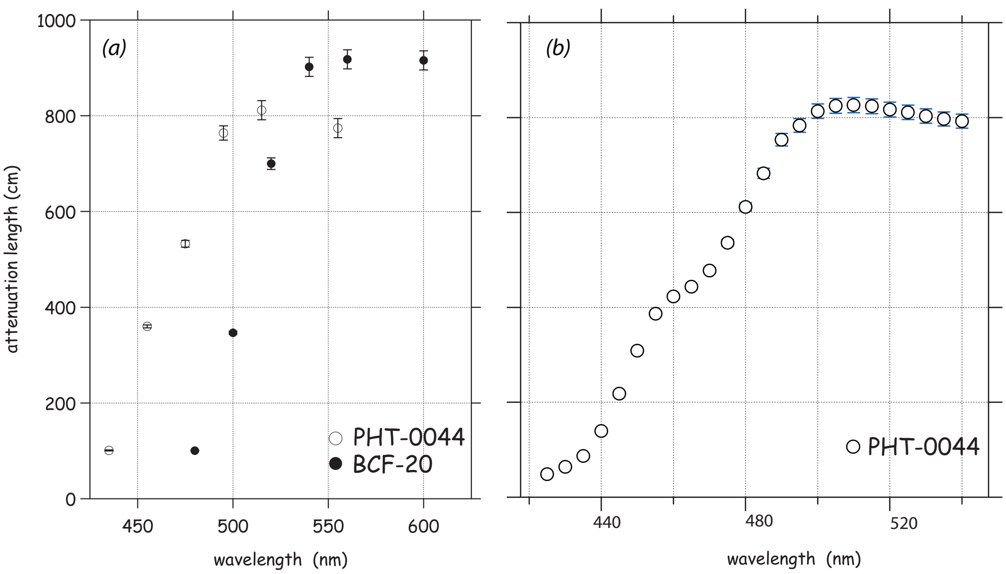

Fig. 7. (a) The attenuation length as a function of wavelength for the PHT-0044 and BCF-20 fibres. The attenuation length is the parameter λ as defined in Eq. 2 and is obtained by fitting the data shown in Fig. 6. (b) The attenuation length as a function of wavelength as extracted by plotting the value of the Moyal fit function as a function of distance at discrete wavelengths and fitting to an exponential. Note the structure in this dependence around 460 nm.

Fig. 4. This is a persistent feature and not an artifact of our measurements or the spectro-photometer response, and shows faintly in the left panel of Fig. 7

due to the lower resolution in that method.

3.3 Fibre spectral shape details

The spectral shapes of the PHT-0044 and BCF-20 fibres differ significantly, as can be seen in Fig. 4. The striking difference between the PHT-0044 and BCF-20 fibres in terms of the loss of light from the source to 8 cm distance is illustrated in a graphical manner in Fig. 8. In that figure, the d=0 cm and 8 cm spectra are shown as a function of wavelength, normalized at 490 nm and 590 nm for the PHT-0044 and BCF-20 fibres, respectively. The emission spectrum at the source (d = 0 cm) for the PHT-0044 fibre was assumed to follow the emission spectrum for BCF-12 as mentioned previously; that and the source spectrum for BCF-20 were provided by the manufacturer. This normalization was based on a combination of long attenuation length and sufficient intensity at each wavelength. With attenuation lengths of $\sim$800 cm and $\sim$900 cm at 490 nm and 590 nm, respectively, as extracted from Fig. 7, the effect of 8 cm in loss of strength is negligible. In addition, variations in the regions around these values resulted in stable ratios of areas under the spectral shapes, further emphasizing the lack of sensitivity to the exact normalization choice.

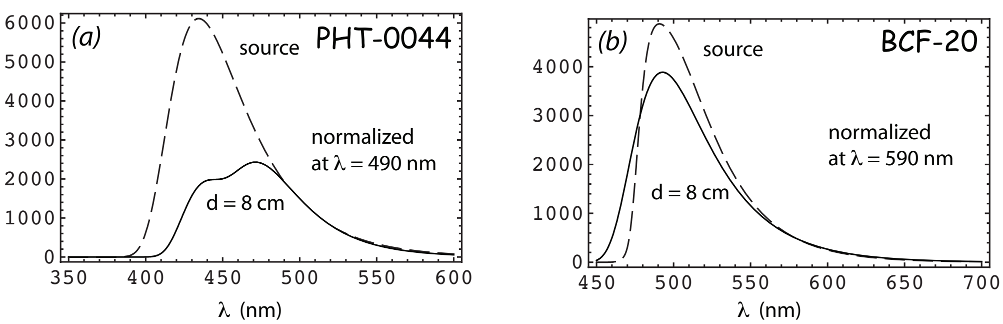

Fig. 8. The manufacturer's d=0 cm source (dashed line) and 8 cm spectra (solid line) are shown, as a function of wavelength for (a) the PHT-0044 and (b) BCF-20 fibres, respectively. Details are presented in the text.

The main features of Fig. 8 are: a) large loss of light from source to 8 cm for PHT-0044 as compared to the BCF-20 fibre and quantified in Section 3.4, and b) a curious discrepancy between the source and 8 cm curves for the BCF-20 is apparent, where the latter extends to lower wavelengths. We have no firm explanation of this, however, a close inspection of the leading edge of the source shows a rather rapid (and unnatural in appearance) rise from its 470 nm base to its 490 nm peak. A possible explanation is that the manufacturer may have used a bandpass filter to block the blue wavelengths of a UV light source.

Our experimental setup used for the measurements, as presented in Section 2, did not allow measurements closer than 8 cm from the source. Therefore, in order to further investigate the double-peaked behavior of the PHT-0044 spectra and to facilitate comparisons to the manufacturer's source spectra, we employed an alternate setup using the laser. In that, the laser light was transported via a clear optical fibre held by a clamp and a lab stand so as to be perpendicular to the tested PHT-0044 fibre, in a manner similar to the LED measurements. In this manner, a short sample (15 cm) of PHT-0044 fibre was tested by coupling it to a clear (BCF-90) 5 cm-long fibre using Q2-3067 optical grease [10], with both fibres positioned in a channel of a plate so as to remain in contact and axially aligned. The clear fibre was threaded and epoxied through a SMA connector and facilitated proximity measurements of the PHT-0044 by bridging the gap from the spectro-photometer's SMA connector to the CCD surface. In this manner, PHT-0044 spectra were collected at distances from 1 to 20 mm in 1 mm steps, from 20 to 60 mm in 5 mm steps and at 100 mm. The latter point provided an "anchor point" to the LED data, since the two measurements had different setups. Indeed, it was reassuring to observe that the LED- and laser-stimulated PHT-0044 spectra at 10 cm were consistent.

Having assured the reliability of the laser measurements, the resultant spectra are shown in Fig. 9, normalized at 500 nm. Normalization at other wavelengths was carried out, but the 500 nm normalization was the most consistent one, since the high-wavelength tails of all distance measurements overlapped perfectly, and no large discrepancies appeared at the two peaks.

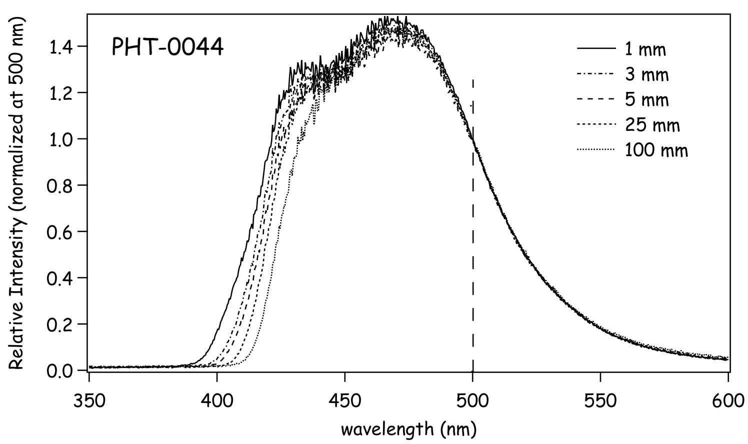

Fig. 9. Measurements from a short sample of PHT-0044 fibre using the UV laser. Spectra were collected at distances from 1 to 20 mm in 1 mm steps, from 20 to 60 mm in 5 mm steps and at 100 mm, but only five of them are shown for reasons of clarity. The spectra were normalized relative to each other at the wavelength value of 500 nm.

The spectra at distances of a few mm's from the excitation source should closely match the "source spectrum" provided by the SciFi manufacturers. For PHT-0044 (and BCF-12), however, the peak emission is listed by them

[10] Dow Corning Corporation, Midland, MI, USA (www.dowcorning.com)

at 435 nm with no evidence of secondary strength at 460-470 nm. Our measurements are in disagreement to those reference spectra: while some strength is evident at 435 nm, the peak emission is at 460-470 nm, instead. One explanation may lie in the attenuation length measurements, shown in Figs. 6 and 7. The attenuation length at 460 nm is $\sim$400 cm, compared to $\sim$80 cm at 435 nm. Thus, if the source spectrum has secondary emission strength around 460-470 nm, the reduced attenuation of the latter compared to the former can result in the double-peak structure observed in our measurements. It is worth noting here that the blue emitting fibres in reference [3], the equivalent fibre types from Kuraray (SCSF-81 and SCSF-81M)[11], and several blue-emitting plastic scintillator data (BC-400, BC-404 and BC-408 from St. Gobain as well as EJ-200 from Eljen[12]) all show a "shoulder" in the source emission spectra in the region of 460-470 nm.

The significant difference in attenuation lengths at 435 nm and 460-470 nm can easily provide the explanation of the structure observed in Fig. 4. However, the attenuation length for 435 nm cannot account for the weak strength observed at a few mm distance from the source location. Another mechanism must be responsible for the suppressed emission at the nominal peak wavelength of 435 nm. Taking into consideration that the reference spectra are generated within scintillation material thickness of 1 cm or more, it is possible that within the 1 mm diameter (maximum effective thickness) of the fibre the UV source does not fully excited the dyes, thus resulting in a reduced strength at the lower wavelengths. The 10 cm distance spectra for BCF-12 in reference [8] appear very similar to those shown in Figs. 4 and **??** of this work. The agreement between the reference spectra and our measurements for BCF-20 further indicates that this effect is indeed confined to lower wavelengths.

A quick calculation from our work shows that the resolving power, $R = \lambda/\Delta\lambda$, of our LED and laser is 28.6 and 375, respectively. Coupled to the aforementioned spectro-photometer resolution of 0.3 nm, these values result in a very fine resolution in wavelength, that does not appear to be the case for the results in reference [9], which is perhaps why the second peak appears to be washed out in their work and other published data.

3.4 Scintillating fibre/photosensor matching

The fibre spectra of intensity versus wavelength in Fig. 10a were convoluted with the spectral response of a typical bi-alkali PMT (the XP2020[13]) and a

[11] Kuraray America Inc., Houston, TX, USA (www.kuraray-am.com)
[12] Eljen Technology, Sweetwater, TX, USA (www.eljentechnology.com)
[13] PHOTONIS SAS, Brive, France (www.photonis.com).

SiPM (the A35H SiPM[14]) in Fig. 10b, respectively, resulting in the curves shown in Fig. 10c and Fig. 10d.

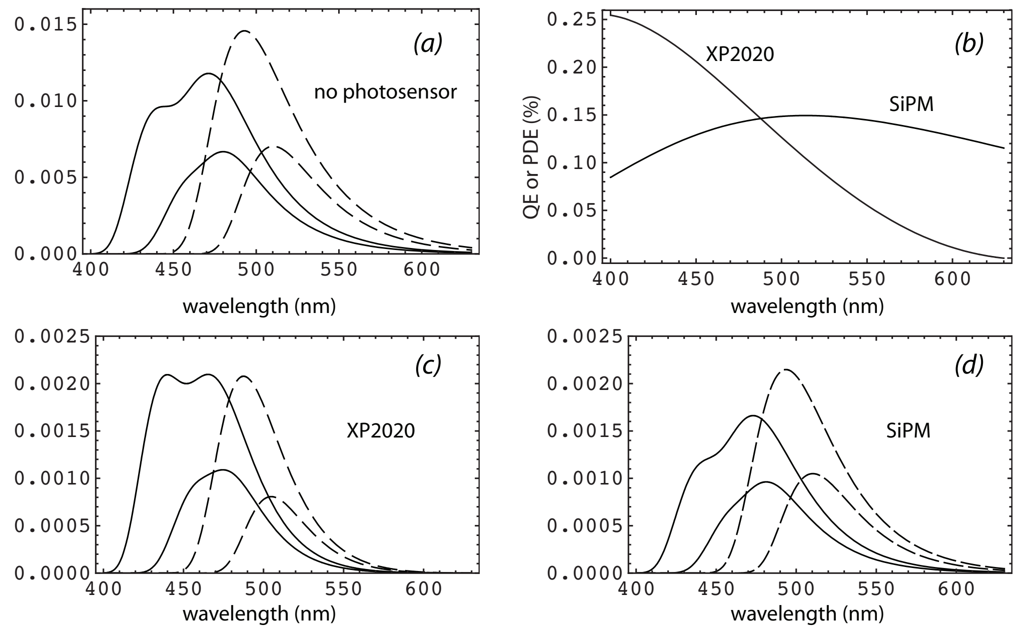

Fig. 10. (a) Emission spectrum for the PHT-0044 (solid lines) and BCF-20 fibres (dashed lines) at 8 cm and 390 cm. The 8 cm spectra for both the blue and green fibres were normalized to give unity for the respective total integrals. (b) The QE and PDE for the XP2020 and SiPM respectively. (c) The PHT-0044 and BCF-20 spectra now convoluted with the QE of the XP2020. Note that the areas under the curves for the 8 cm distance are set to 1.0 in plot (a), which results in areas under the PHT-0044 spectra of 0.164 and 0.068 while those under the BCF-20 curves are 0.110 and 0.040, both in plot (c). (d) Similar curves, but now convoluting with the PDE of the SiPM. The areas under the PHT-0044 curves are 0.136 and 0.067 while for the BCF-20 curves we have 0.145 and 0.065.

Specifically, the PHT-0044 and BCF-20 spectra were convoluted over wavelength with the XP2020 QE and SiPM PDE, respectively, and were plotted as a function of distance from the source. Double-exponential fits were employed with two attenuation lengths (short and long). Note that when the PHT-0044 spectrum is folded with the XP2020 QE, the fraction of the integrated source intensity (see Fig. 8a) seen at 200 cm from the source is 24% while the corresponding fraction for the BCF-20 with the A35H is 61%. Since the QE and PDE are relatively flat in the region of interest, these fractions reasonably describe the actual loss of light in the fibres. One can conclude that, whereas the integrated intensity of the PHT-0044 fibre coupled to the XP2020 is superior to that of the BCF-20 fibre, the results are indistinguishable when the fibres are coupled to the SiPM, only if one considers the data in the d = 8-380 cm region, and not from the source.

[14] A prototype SiPM from SensL with a 35μm pixel pitch.

The wavelength-averaged QE of the XP2020 and PDE of the A35H SiPM were computed using the emission spectra of PHT-0044 and BCF-20. The integrals of these spectra over wavelength were computed as a function of distance, with and without convolution with the QE (or PDE), by dividing the integral with convolution by the integral without convolution. The results are shown in Fig. 11. For PHT-0044, at 200 cm from the source, the average QE of the XP2020 is 15% and that of the A35H is 14%. For BCF20, at 200 cm from the source, the average QE of the XP2020 is 9% and that of the A35H is 14%.

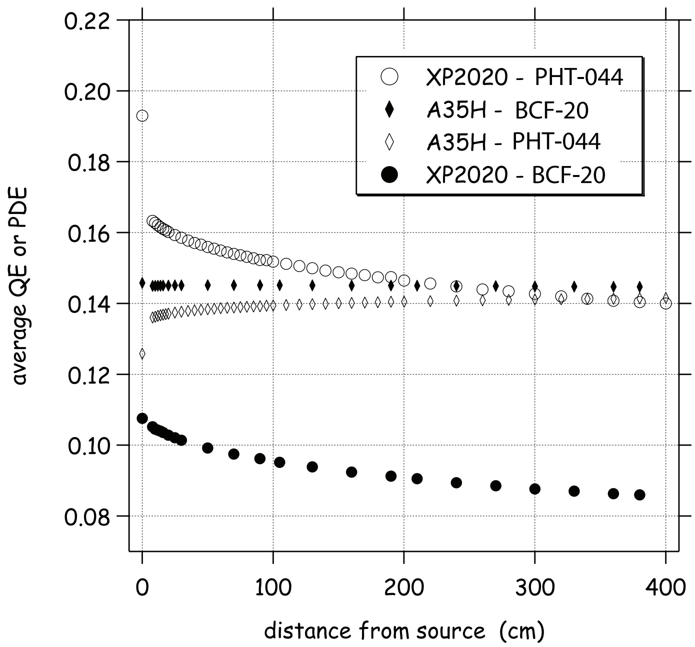

Fig. 11. The average QE of the XP2020 and the average PDE of the A35H, as a function of distance from source for PHT-0044 and BCF-20 scintillating fibres, are shown. Details are given in the text.

3.5 Attenuation length with and without photosensor

As can be seen in Fig. 6. the light output of a fibre is strongly dependent on λ and d, with shorter wavelengths that dominate at small distances being replaced by longer wavelengths at larger distances. However, the bulk attenuation is the result of the integrated light yield and, being the convolution of two different response regions, cannot be effectively represented by a single exponential function. Therefore, each fibre was characterized by [11]:

$$I(d) = I_0 + \alpha_1 \cdot e^{-(d-d_0)/\lambda_1} + \alpha_2 \cdot e^{-(d-d_0)/\lambda_2} \tag{3}$$

The values from this fit are shown in Table 1. Using this information, the attenuation length for PHT-0044 and BCF-20 was plotted with and without the photosensor coupling in Fig. 12. The weighted attenuation length in that table is based on the relative amplitudes of the two exponentials.

The long bulk attenuation length of 414 cm for the PHT-0044 fibre combined with the XP2020 agrees well with the specification supplied by the manufacturer, which was extracted using a ^{90}Sr electron source and a bi-alkali vacuum PMT. Those measurements were made between 64 cm and 200 cm and are dominated by the long component [15] . For the BCF-20 fibre, on the other hand, the manufacturer's specification was derived using bi-alkali PMT's and our results cannot be compared directly to those. However, the smoothly varying and relatively flat QE response of a PMT over the emission spectrum of BCF-20 (approximately 460 nm to 560 nm; see Figs. 10b and 11) will not alter the weighted attenuation length of 408 cm, and St. Gobain quotes a value larger than 350 cm. In conclusion, our measurements using UV light sources and a spectral deconvolution agree very well with the manufacturer's ones using an electron source, once the range of distance measurements are taken into consideration.

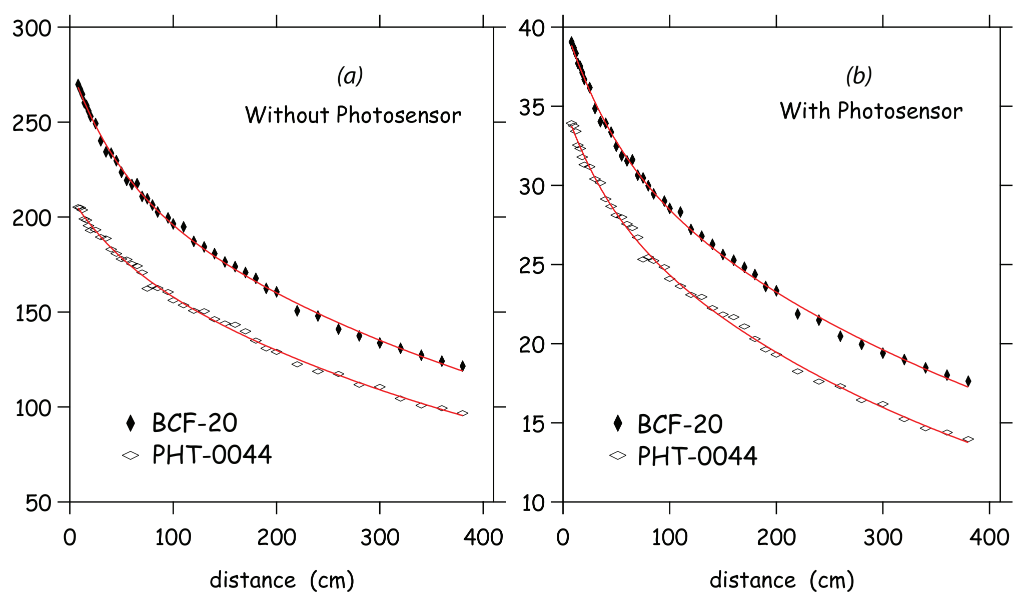

Fig. 12. Double-exponential fits to the PHT-0044 and BCF-20 data without and with the convolution of the photosensor. The photosensor in the case of PHT-0044 is the XP2020 and in the case of BCF20 is the SiPM. The results of the fits are shown in Table 1.

[15] Information provided formerly by PolHiTech (www.polhitech.it)

4 Summary and Conclusions

The relevant quantities in matching SciFi's to photosensors are the emission spectra of the former and the spectral response of the latter because this combination affects the number of photoelectrons generated independent from attenuation length. Changes in the spectral emission of the fibre with length affects the number of photoelectrons detected and introduces a non-linearity in the energy response of the detector system. The combination of SiPM's and fast green emitting SciFi's, such as BCF-20, in applications where the technology of the latter is relevant, is an optimal one due to the flat PDE response of the SiPM in the emission wavelength spectrum of the former and the stability of the peak emission wavelength of the SciFi, as seen in Fig. 10. Such combinations have already been reported in the literature [12].

Fast blue SciFi's are by far the most widely used fibres, in combination with bi-alkali type of vacuum PMTs. Most such fibres with peak emission at nominal 435 nm – examples of which are PHT-0044 (now not available anymore), BCF-12 and SCSF-81 – share very similar attenuation lengths and spectral functions. However, our testing of several different samples produced consistent emission spectra that are quite different than the manufacturers specifications. In this paper we have shown only the results for PHT-0044 due to the large detailed amount of experimentation that we have done with that particular fibre. The peak emission is not at 435 nm, which appears only as a secondary bump, but at approximately 470 nm, instead. One possible explanation is that the thickness of the fibre presented to the exciting UV light (maximum 1 mm) is not adequate to absorb the UV light and to allow its full conversion to the emission spectrum representative of the material in sufficient thickness. As such, the emission spectra in this paper near the illumination center, shown in Fig. 9, are the effective spectra for such types of fibres.

This observation leads to question the effective photon yield listed by most manufacturers of approximately 8,000 photons/MeV of deposited energy by minimum ionizing particles (MIP). If such yield is the integral of the full emission spectrum, as listed in the product literature, then a significant fraction, approaching 50%, is not available for excitation by UV light, as shown in Fig. 9. Experimental results are consistent with such reduced photon yields. BCAL data with cosmic rays and photon beams verify that the nominal photon yield of 8,000/MeV has to be reduced by a significant fraction, over and above that justified by attenuation length and spectral distortion with distance, to account for the measured yield of 660 photoelectrons at 1 GeV incident photons [13]. The same treatment was applied to the KLOE results of 700 photoelectrons also at 1 GeV [10], taking into consideration the single-clad fibres used and the very efficient light guide-Winston Cone collectors used.

The conclusion derived here is that that our work explains the physics cause for the commonly known fact that the measured number of photoelectrons from SciFis do not reflect the manufacturers' number for scintillating material of 8,000/MeV. The actual number is closer to around 4,000 photons/MeV at the scintillation location for 1 mm diameter blue emitting fibre.

Using the methodology described in this paper, it is concluded that the conversion of UV light in 1 mm of green (BCF-20) material is much more efficient than for blue fibres. The overlap of the reference and measured spectra in Fig. 8 is significant, indicating a small loss of photon yield due to conversion to the final emission spectrum. If this also represents the case of charged particle tracks in BCF-20 fibres, as the results for PHT-0044 indicate, then one expects a factor of approximately 2.5 times the photoelectron yield of the BCF-20/SiPM combination than obtained with the PHT-0044/PMT combinations.

It would be advisable for the manufacturers of scintillating fibres to show actual spectra obtained in such thin materials, rather than reference emission spectra than can only be realized in thicknesses beyond the realm of fibre use and availability and to quote the effective number of photons per MeV of energy deposit (MIP) produced in fibres.

Finally, the attenuation lengths of both PHT-0044 and BCF-20 are in good agreement with specifications if the measurements duplicate the manufacturers methodology. As such, both blue and green SciFi's exhibit comparable bulk attenuation lengths with or without the influence of the two corresponding types of photosensors used in our work.

5 Acknowledgments

This work was supported by NSERC grant SAPJ-326516 and DOE grant DE-FG02-0SER41374 as well as Jefferson Science Associates, LLC. under U.S. DOE Contract No. DE-AC05-06OR23177. Finally, many thanks must be given to Alex Dzierba who contributed immensely to the analysis and writing of this paper.

	Without Photosensor		With Photosensor	
Component	PHT-0044	BCF-20	PHT-0044	BCF-20
short (cm)	50±14	48±8	43±8	50±9
long (cm)	478±21	481±21	414±14	491±21
weighted (cm)	428±23	400±23	353±18	408±25

Table 1
Short and long attenuation length components for the PHT-0044 and BCF-20 fibres, as extracted from a double-exponential fit. The weighted attenuation length is based on the relative amplitudes of the two exponentials. The photosensor in the case of PHT-0044 is the XP2020 and in the case of BCF-20 is the SiPM.

Figure Captions

Fig. 1. Emission and absorption spectra from the secondary dye of (a) BCF-12 and (b) BCF-20 fibres. Also shown are the stimulated wavelength ranges from the 373 nm LED and 375 nm laser used in our measurements, as discussed below. All curves have been arbitrarily normalized to facilitate the comparison of their spectral shapes. (colour online)

Fig. 2. Comparison of the emission spectra of the LED and the laser as measured directly, using the spectro-photometer, and plotted on a logarithmic scale. Details are provided in the text. (colour online)

Fig. 3. Schematic drawing of the experiment. The test fibre is shown as the bold horizontal line: on the right it is clamped to a lab stand (C), in the middle it threads through the legs of the LED support stand via barrels (B) having 1 mm inner diameter holes and external threads that mount on the support frame and on the left it is connected to the slave channel (S) of the SD2000 spectro-photometer by an SMA connector. The SD2000 connects to the ADC via a flat-ribbon bus and the ADC, in turn, connects to a PC via a USB cable. The vertical arrow pointing downwards from the LED housing indicates the direction of the incident light through its port (P) onto the test fibre. The horizontal displacement of the light direction to the entrance of the SD2000 master channel is our distance parameter, z. This figure is not to scale: for example, the LED's port is a lot closer to the fibre than implied in this schematic.

Fig. 4. The results of fits to Moyal functions for spectral measurements at source distances ranging from 8 to 380 cm for (a) PHT-0044 and (b) BCF-20 fibres. The wavelength ranges labeled A through F in the plots will be referenced later in this paper. (colour online)

Fig. 5. Dependence of the Moyal fit parameters (a) μ and (b) σ as a function of source distance for the PHT-0044 and BCF-20 fibres.

Fig. 6. Integrals of the Moyal fits to the fitted data are shown as a function of source distance for (a) the PHT-0044 and (b) the BCF-20 fibres. The points labeled A through F are the integrals for the wavelength ranges defined in Fig. 4. The curves are results of fits to a single exponential. More details are given in the text.

Fig. 7. (a) The attenuation length as a function of wavelength for the PHT-0044 and BCF-20 fibres. The attenuation length is the parameter λ as defined in Eq. 2 and is obtained by fitting the data shown in Fig. 6. (b) The attenuation length as a function of wavelength as extracted by plotting the value of the Moyal fit function as a function of distance at discrete wavelengths and fitting

to an exponential. Note the structure in this dependence around 460 nm.

Fig. 8. The manufacturer's d=0 cm source (dashed line) and 8 cm spectra (solid line) are shown, as a function of wavelength for (a) the PHT-0044 and (b) BCF-20 fibres, respectively. Details are presented in the text.

Fig. 9. Measurements from a short sample of PHT-0044 fibre using the UV laser. Spectra were collected at distances from 1 to 20 mm in 1 mm steps, from 20 to 60 mm in 5 mm steps and at 100 mm, but only five of them are shown for reasons of clarity. The spectra were normalized relative to each other at the wavelength value of 500 nm.

Fig. 10. (a) Emission spectrum for the PHT-0044 (solid lines) and BCF-20 fibres (dashed lines) at 8 cm and 390 cm. The 8 cm spectra for both the blue and green fibres were normalized to give unity for the respective total integrals. (b) The QE and PDE for the XP2020 and SiPM respectively. (c) The PHT-0044 and BCF-20 spectra now convoluted with the QE of the XP2020. Note that the areas under the curves for the 8 cm distance are set to 1.0 in plot (a), which results in areas under the PHT-0044 spectra of 0.164 and 0.068 while those under the BCF-20 curves are 0.110 and 0.040, both in plot (c). (d) Similar curves, but now convoluting with the PDE of the SiPM. The areas under the PHT-0044 curves are 0.136 and 0.067 while for the BCF-20 curves we have 0.145 and 0.065.

Fig. 11. The average QE of the XP2020 and the average PDE of the A35H, as a function of distance from source for PHT-0044 and BCF-20 scintillating fibres, are shown. Details are given in the text.

Fig. 12. Double-exponential fits to the PHT-0044 and BCF-20 data without and with the convolution of the photosensor. The photosensor in the case of PHT-0044 is the XP2020 and in the case of BCF20 is the SiPM. The results of the fits are shown in Table 1.

References

[1] GlueX/Hall D Collaboration, The Science of Quark Confinement and Gluonic Excitations, GlueX/Hall D Design Report, **Ver.4** (2002). (http://www.phys.cmu.edu/halld).

[2] A.R. Dzierba, C.A. Meyer and E.S. Swanson, American Scientist, **88**, 406 (2000).

[3] A.J. Davis *et al.*, Nucl. Instr. and Meth. A 276 (1989) 347.

[4] Yu.G. Kudenko, L.S. Littenberg, V.A. Mayatski, O.V. Mineev and N.V. Yershov, Nucl. Instr. and Meth. A 469 (2001) 340.

[5] C.P. Achenbach, arXiv:nucl-ex/0404008 v1, (2004).

[6] R.C. Ruchti: Ann. Rev. Nucl. Part. Sci. 46 (1996) 281.

[7] J. E. Moyal, *Phil. Mag.* 46 (1955) 263.

[8] G. Drexlin, V. Eberhard, D. Hunkel and B. Zeitnitz, Nucl. Instr. and Meth. A 360 (1995) 245.

[9] L. Archambault *et al.*, Med. Phys. 32 (7) (2005) 2271.

[10] A. Antonelli *et al.*, Nucl. Instr. and Meth. A 370 (1996) 367.

[11] K.V. Alexandrov *et al.*, Nucl. Instr. and Meth. A 459 (2001) 123.

[12] H. Gast et al., arXiv:0711.4694v1 [physics.ins-det] 29 Nov 2007.

[13] B.D. Leverington *et al.*, GlueX-doc-1071-v1 (http://portal.gluex.org/, Documents, Public), Technical Report, GlueX Collaboration, 2007; submitted to Nucl. Instr. and Meth. A (2008).